Supporting Information

Toward stretchable batteries: 3D-printed deformable electrodes and separator enabled by nanocellulose

Ji Qian[1,2,‡], Qiongyu Chen[1,‡], Min Hong[2], Weiqi Xie[1], Shuangshuang Jing[2], Yinhua Bao[1], Gang Chen[2], Zhenqian Pang[1], Liangbing Hu[2], Teng Li[1,]*

[1]Department of Mechanical Engineering, University of Maryland, College Park, Maryland, 20742 USA

[2]Department of Materials Science and Engineering, University of Maryland, College Park, Maryland, 20742 USA

[*] Email: lit@umd.edu

[‡] These authors contributed equally to this work.

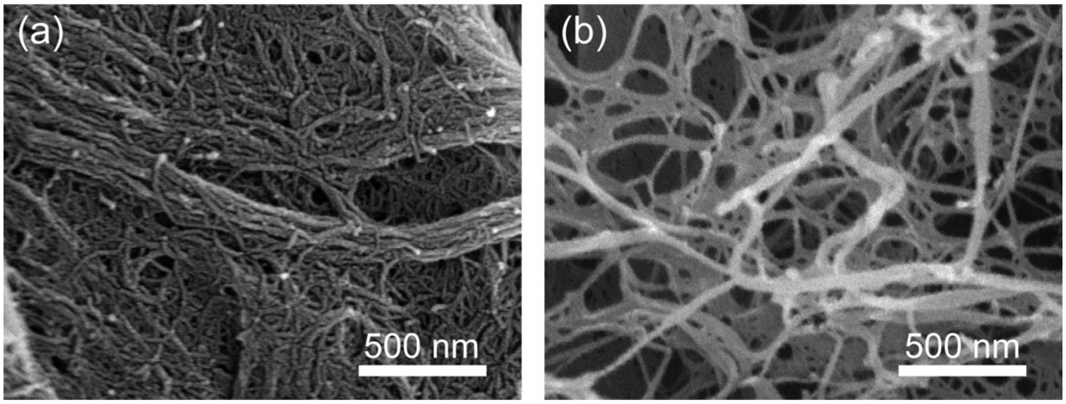

Figure S1. SEM images of (a) CNTs and (b) NFC obtained by freeze-drying.

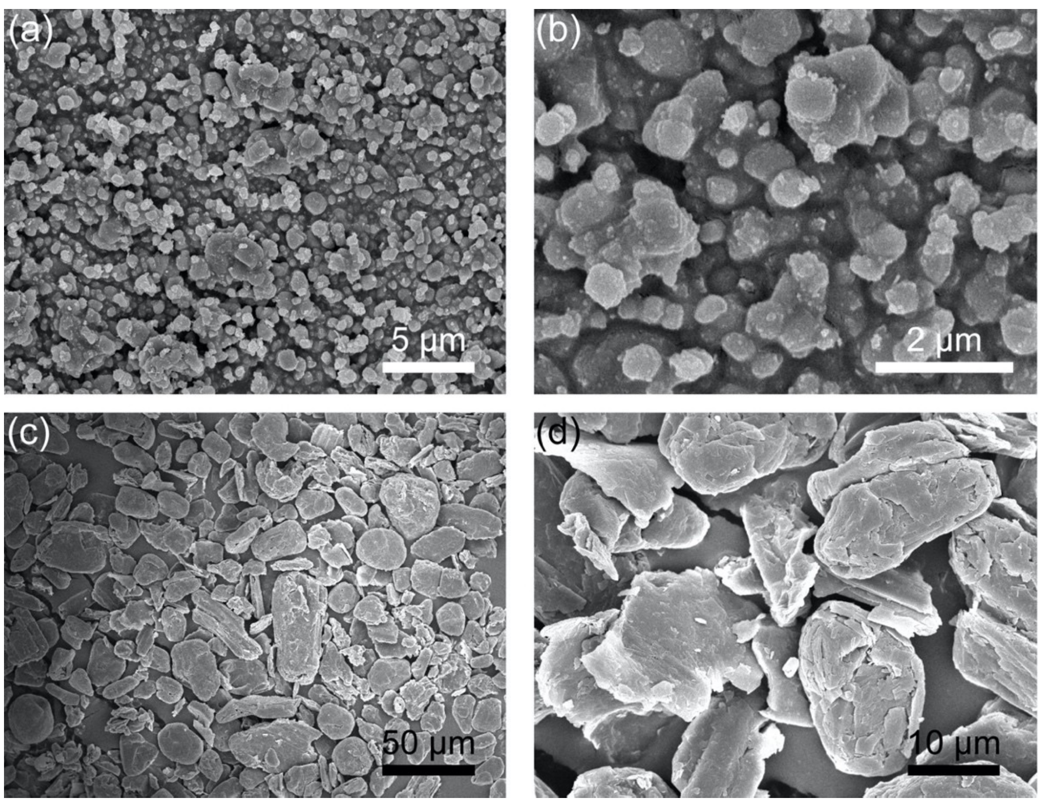

Figure S2. SEM images of (a, b) LFP and (c, d) graphite powders.

Figure S3. Photos of the CNTs dispersed in water without (left) or with (right) NFC.

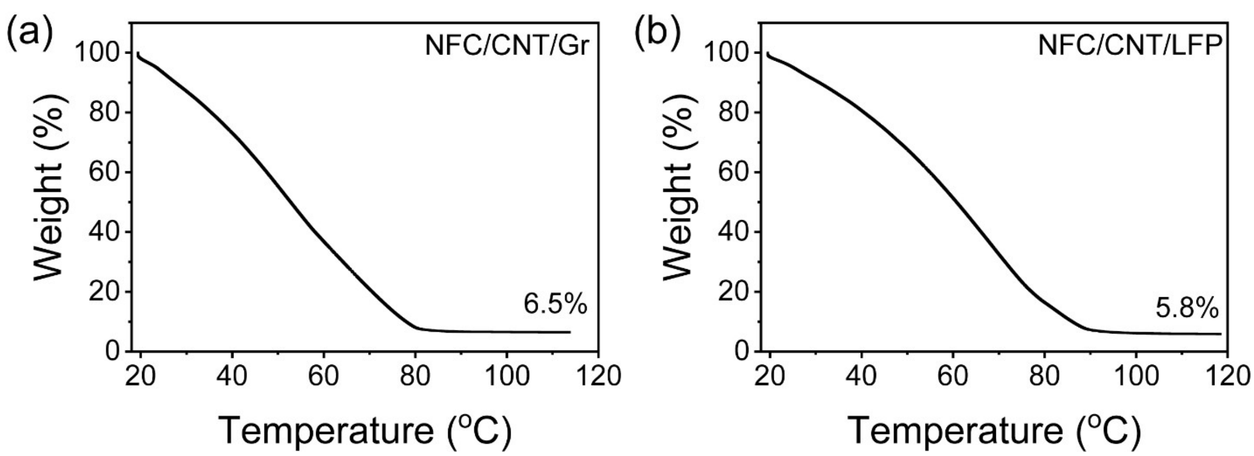

Figure S4. TGA curves of the NFC/CNT/Gr and NFC/CNT/LFP inks.

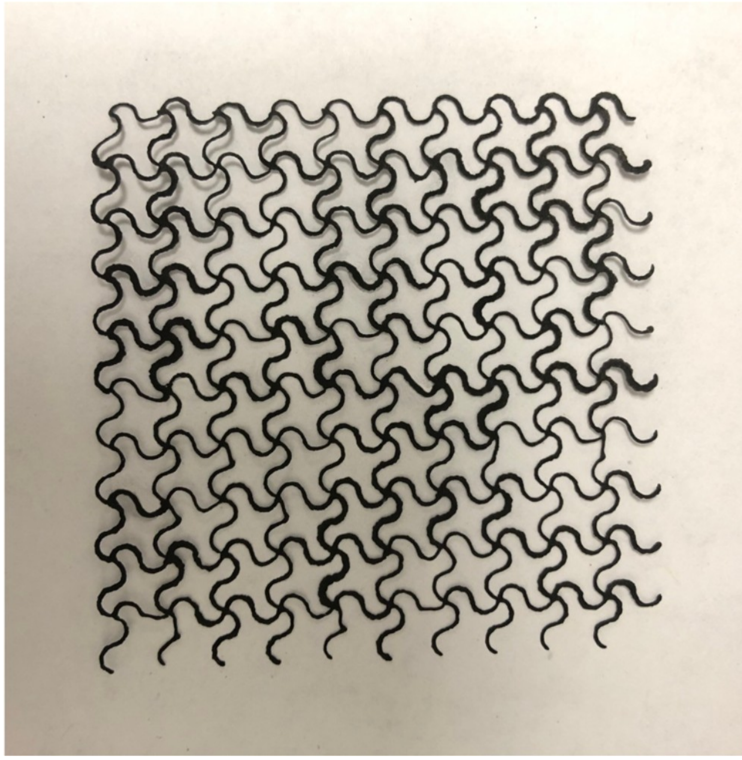

Figure S5. Photo image of a 3D-printed NFC/CNT/Gr electrode with a size of 60 mm × 60 mm.

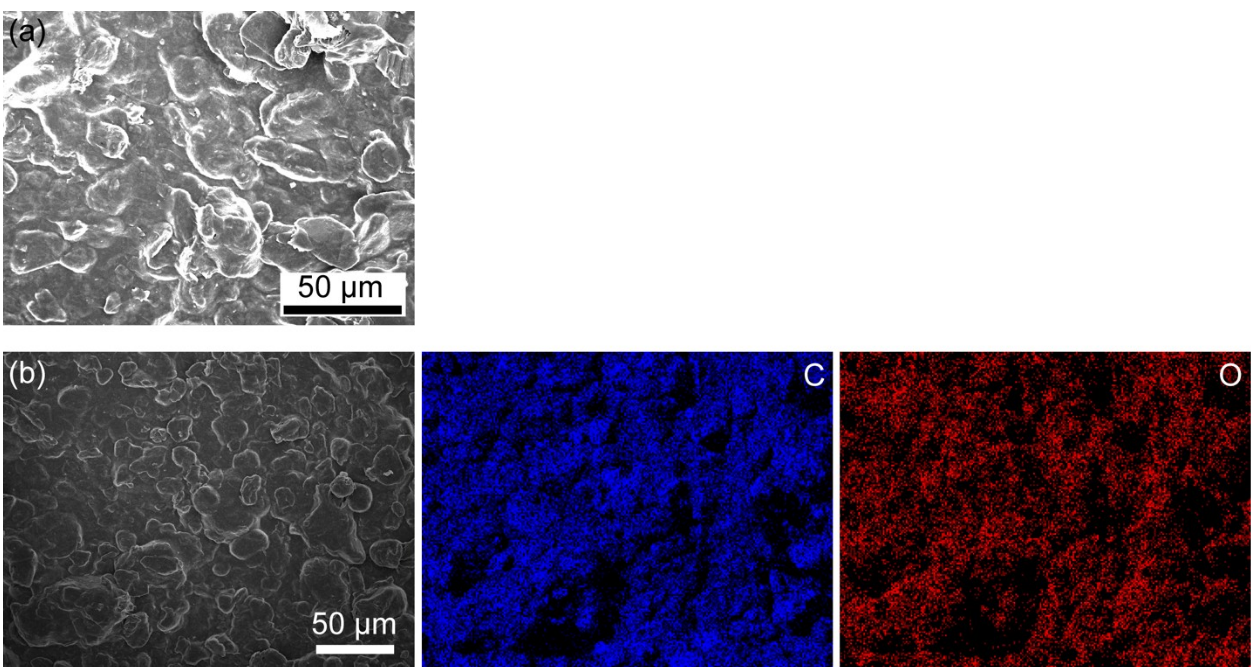

Figure S6. (a) SEM image of NFC/CNT/Gr electrode and (b) the EDS elemental mapping.

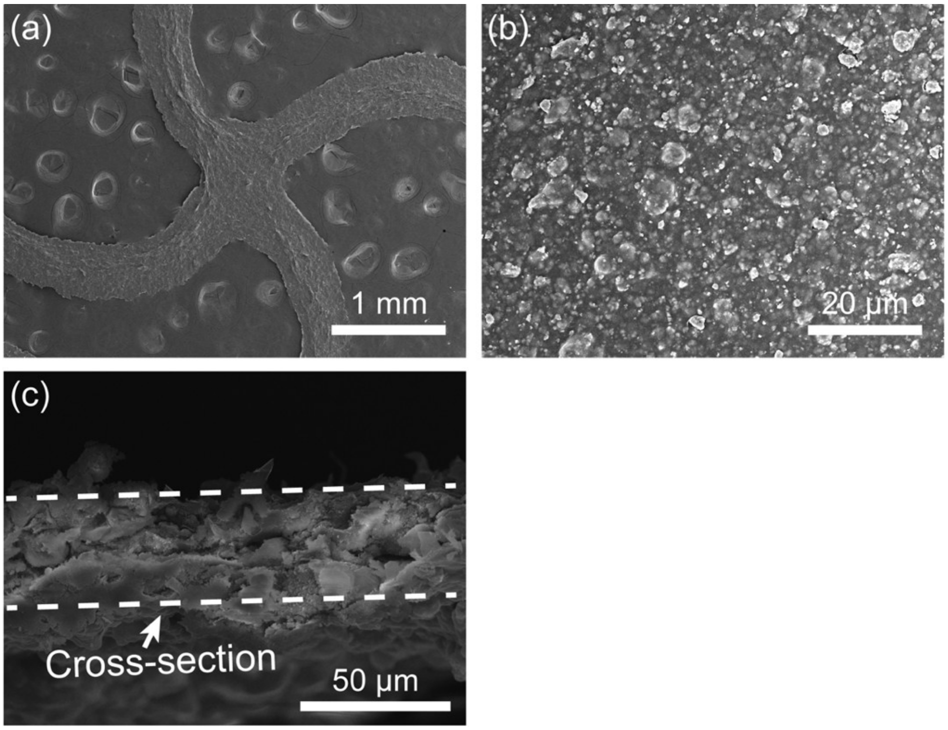

Figure S7. (a) Photo of the prepared NFC/CNT/LFP electrode. (b-d) Top-view and (e, f) cross-sectional SEM images of NFC/CNT/LFP electrode with different magnifications.

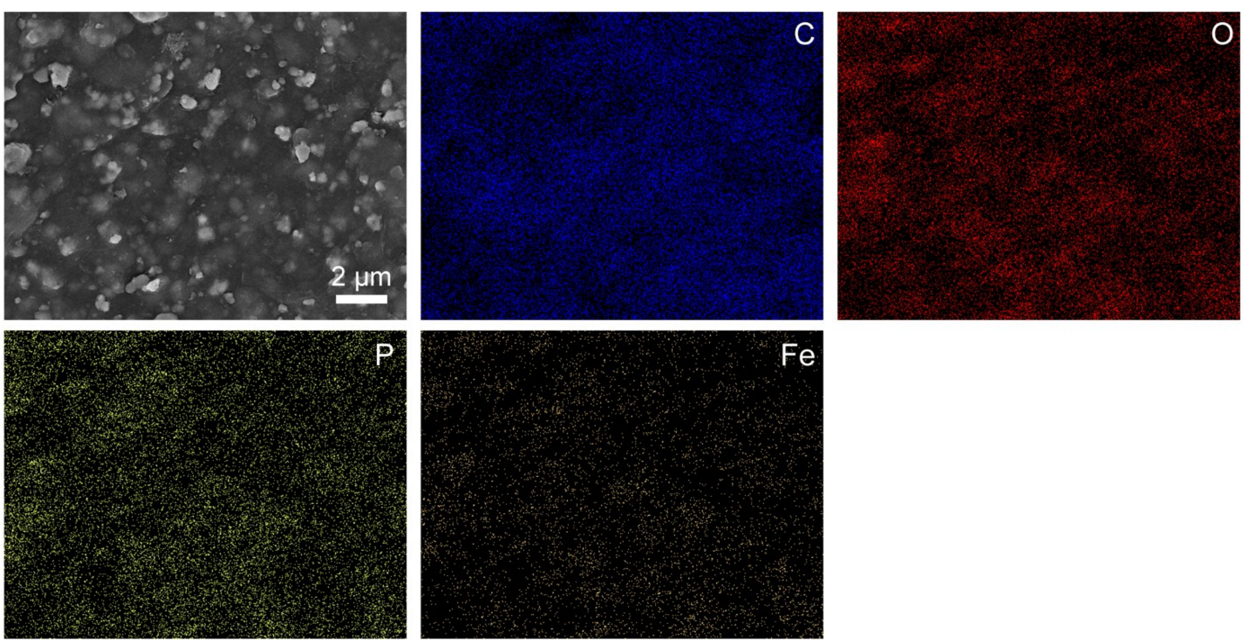

Figure S8. SEM image of NFC/CNT/LFP electrode and corresponding EDS elemental mapping.

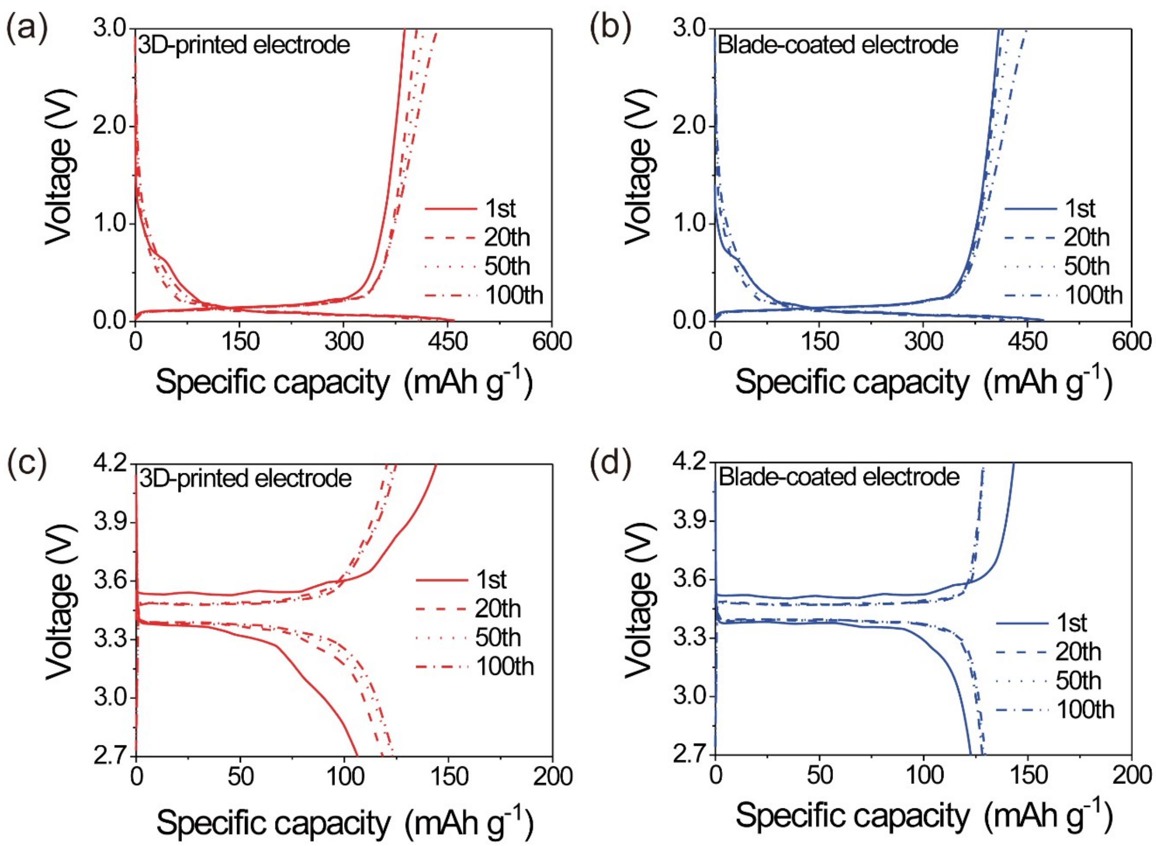

Figure S9. Comparison of the discharge-charge profiles between 3D-printed and conventional blade-coated electrodes: (a,b) Gr anodes and (c,d) LFP cathodes.

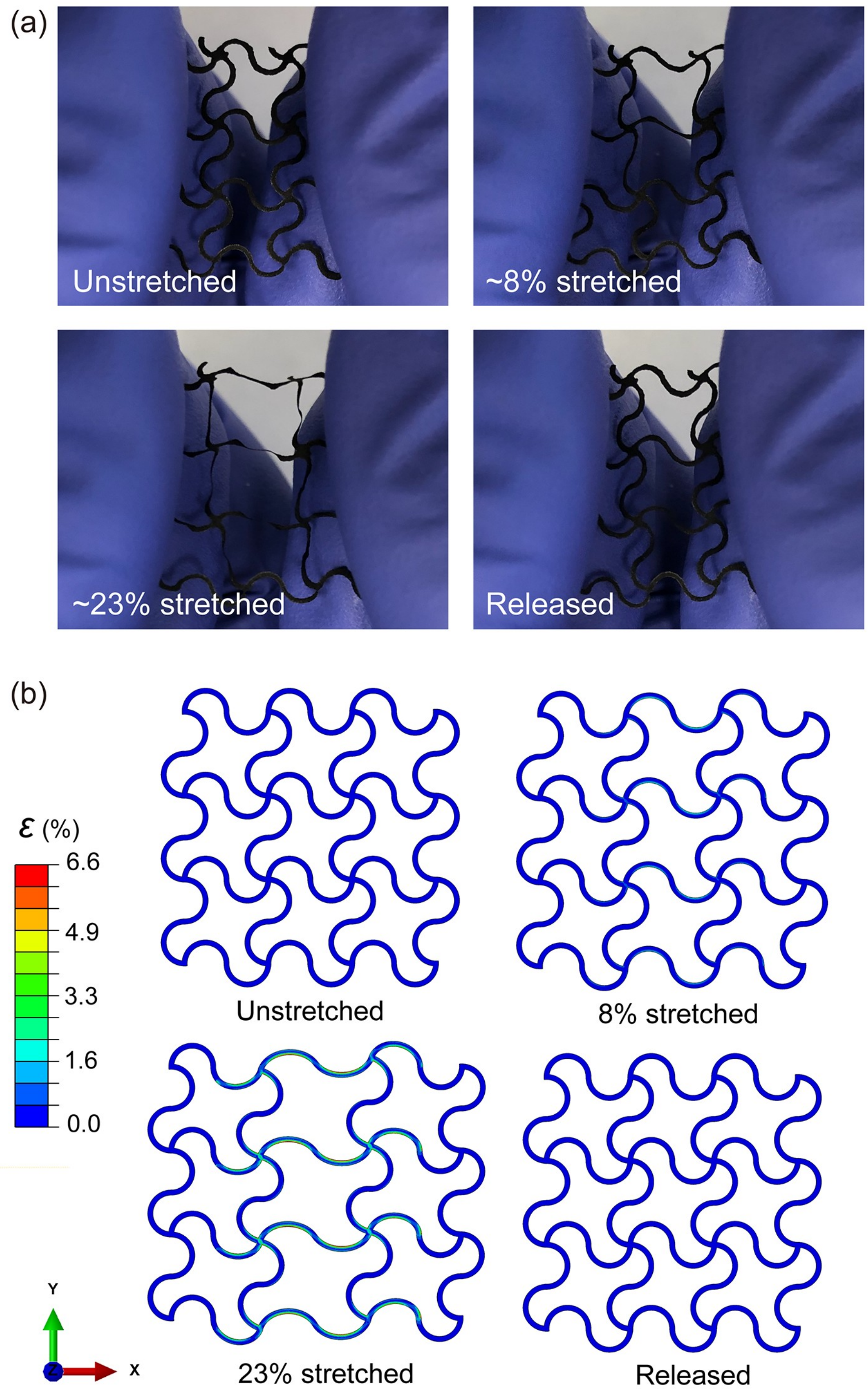

Figure S10. Photos of the NFC/CNT/Gr electrode under different stretched states along the edge direction, and (b) the FEA simulation results at the corresponding stretched states, showing the electrode with a stretchability over 20% along the edge direction.

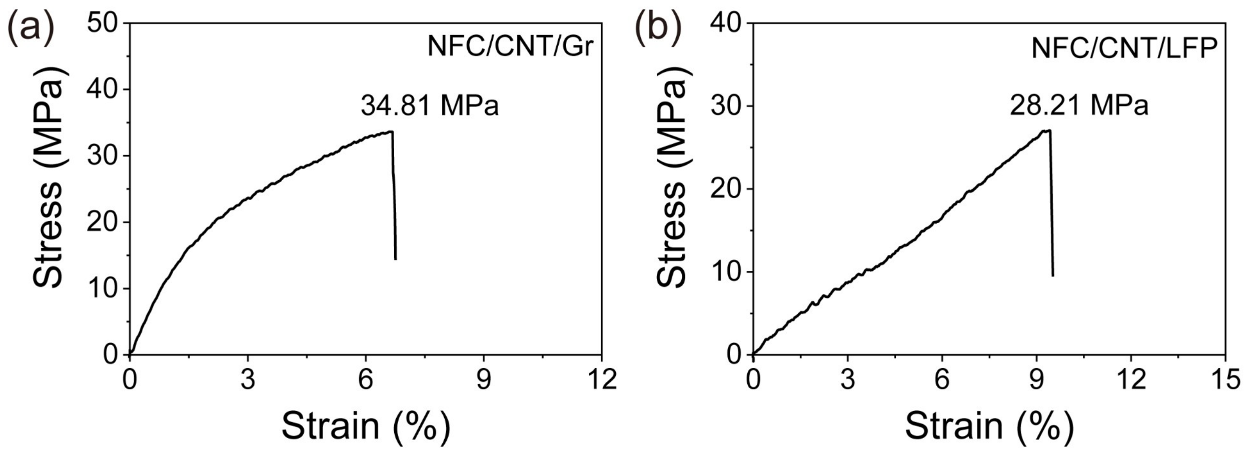

Figure S11. (a) Tensile stress–strain curves of an NFC/CNT/Gr filament, which yields a failure strain of 6.65%, a tensile strength of 34.81 MPa, and a Young's modulus of 1.24 GPa. (b) Tensile stress–strain curves of an NFC/CNT/LFP filament, which yields a failure strain of 9.38%, a tensile strength of 28.21 MPa, and a Young's modulus of 0.32 GPa.

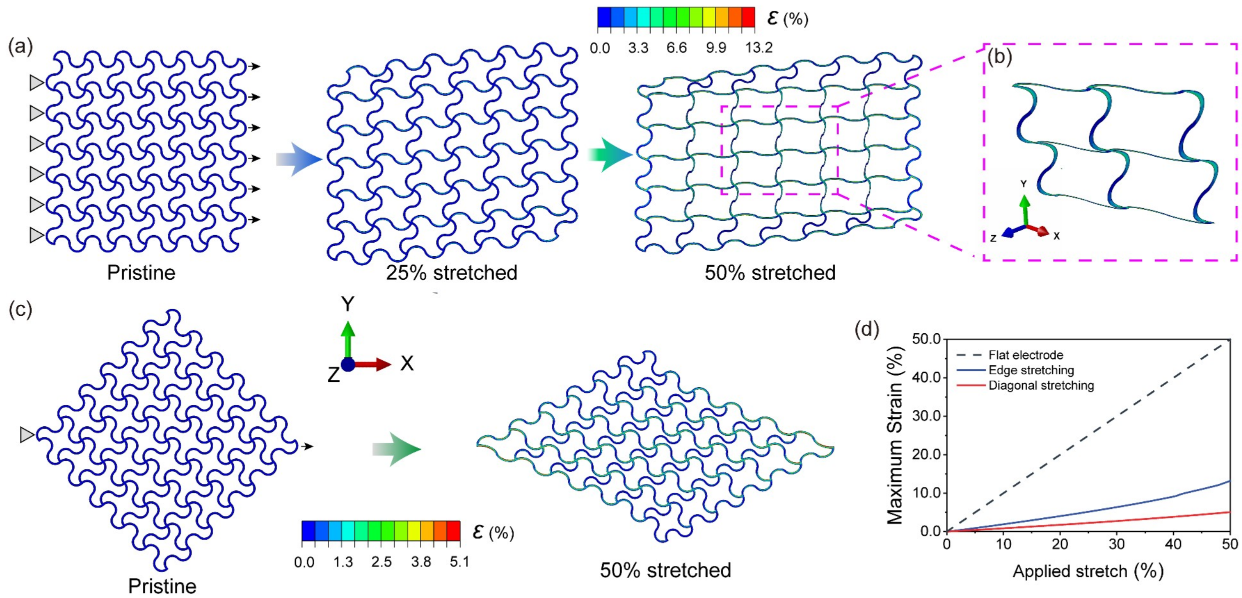

Figure S12. (a) FEA simulation results of the patterned electrode at 25% and 50% stretched states along the edge and (b) the magnified contour plot of the maximum principal strain of the twisted building block at a 50% stretch. (c) FEA simulation results of the pattern electrode stretched along the diagonal direction. (d) The comparison of the maximum principal strain in the conventional flat and 3D-printed patterned electrodes at different stretched states.

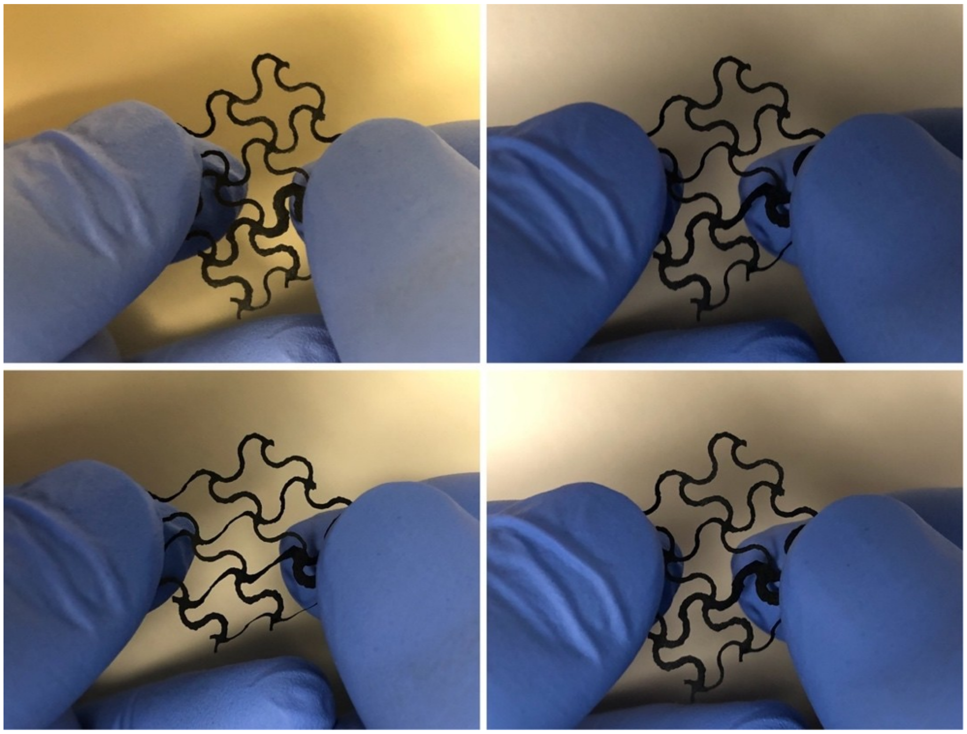

Figure S13. Photos of an NFC/CNT/LFP electrode under different stretched states.

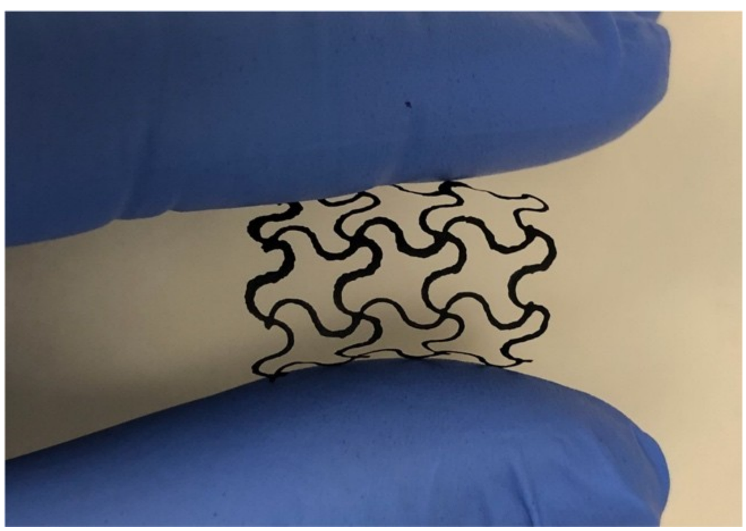

Figure S14. Photos of an NFC/CNT/LFP electrode under the 180° bended state.

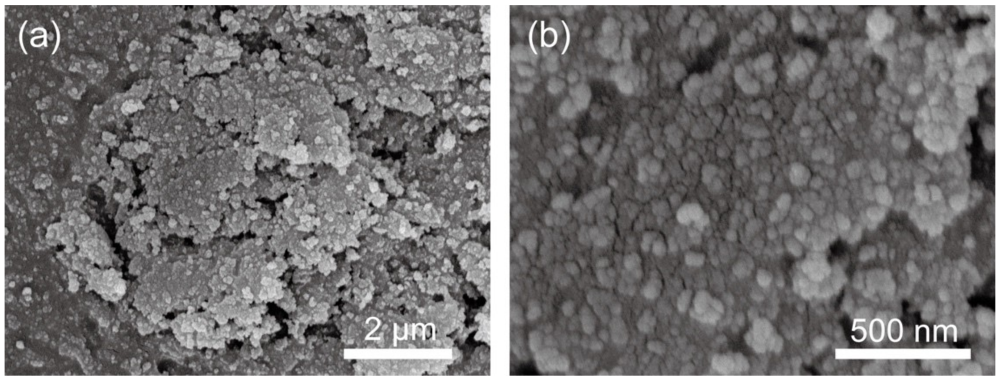

Figure S15. SEM images of nano-Al_2O_3 powders.

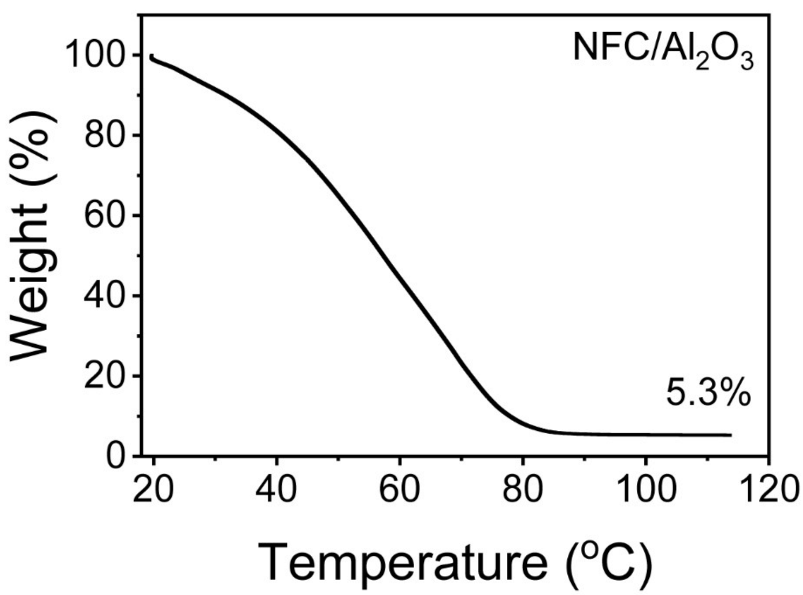

Figure S16. TGA curves of the NFC/Al_2O_3 ink.

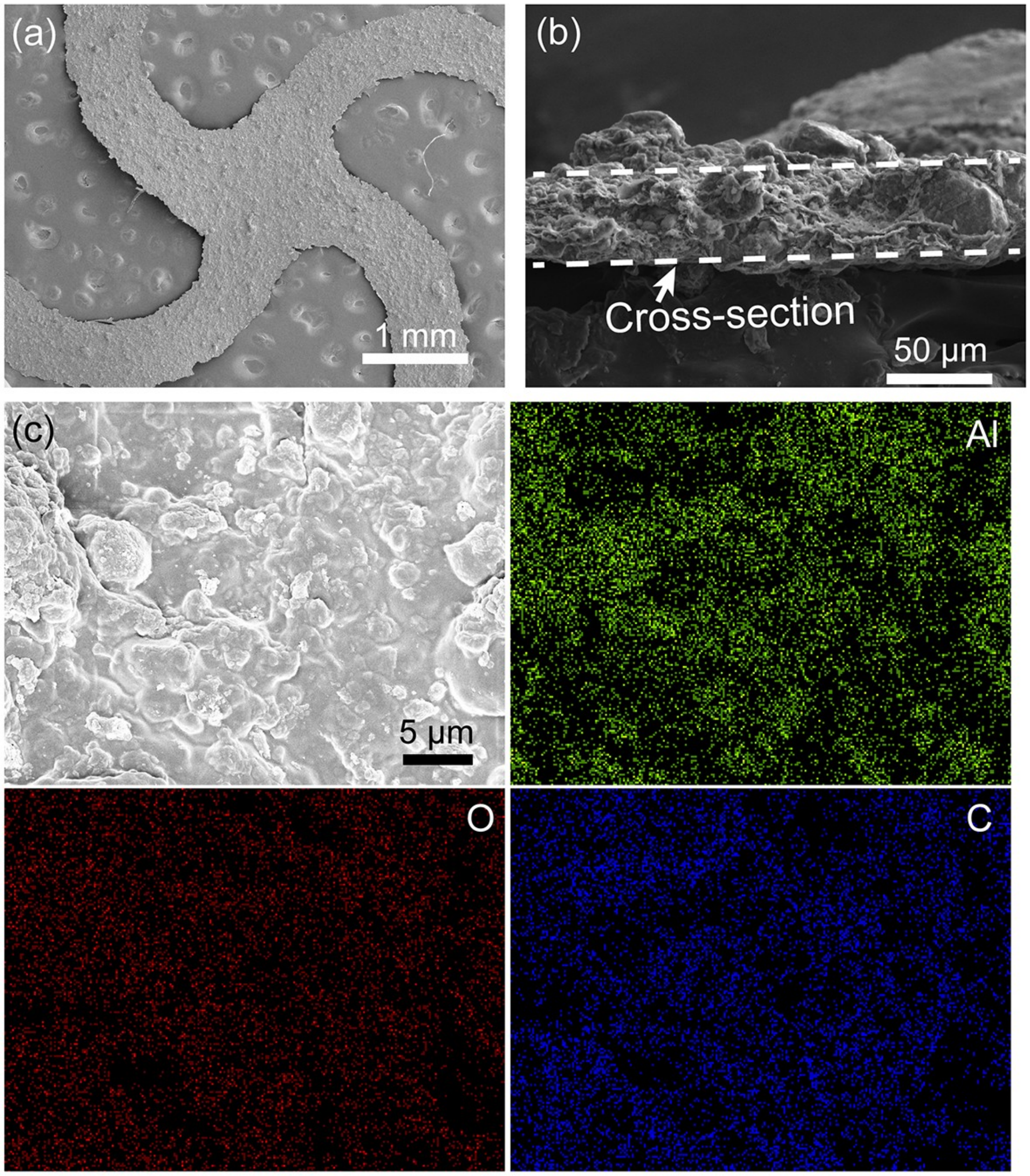

Figure S17. (a) Photo of the prepared NFC/Al_2O_3 separator. (b) Cross-sectional SEM images of NFC/Al_2O_3 separator. (c) Top-view SEM image of NFC/Al_2O_3 separator and corresponding EDS elemental mappings.

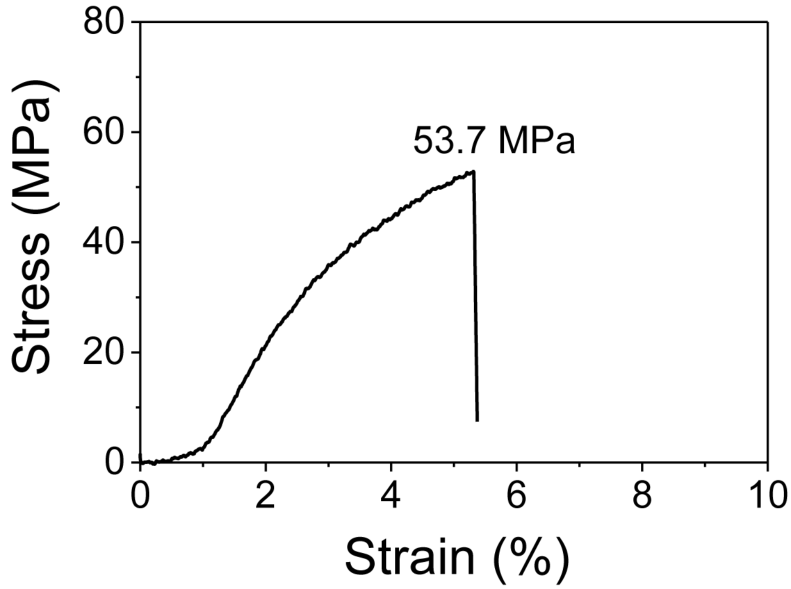

Figure S18. Tensile stress–strain curves of NFC/Al_2O_3, which yields a failure strain of 5.33%, a tensile strength of 53.72 MPa, and a Young's modulus of 1.64 GPa.

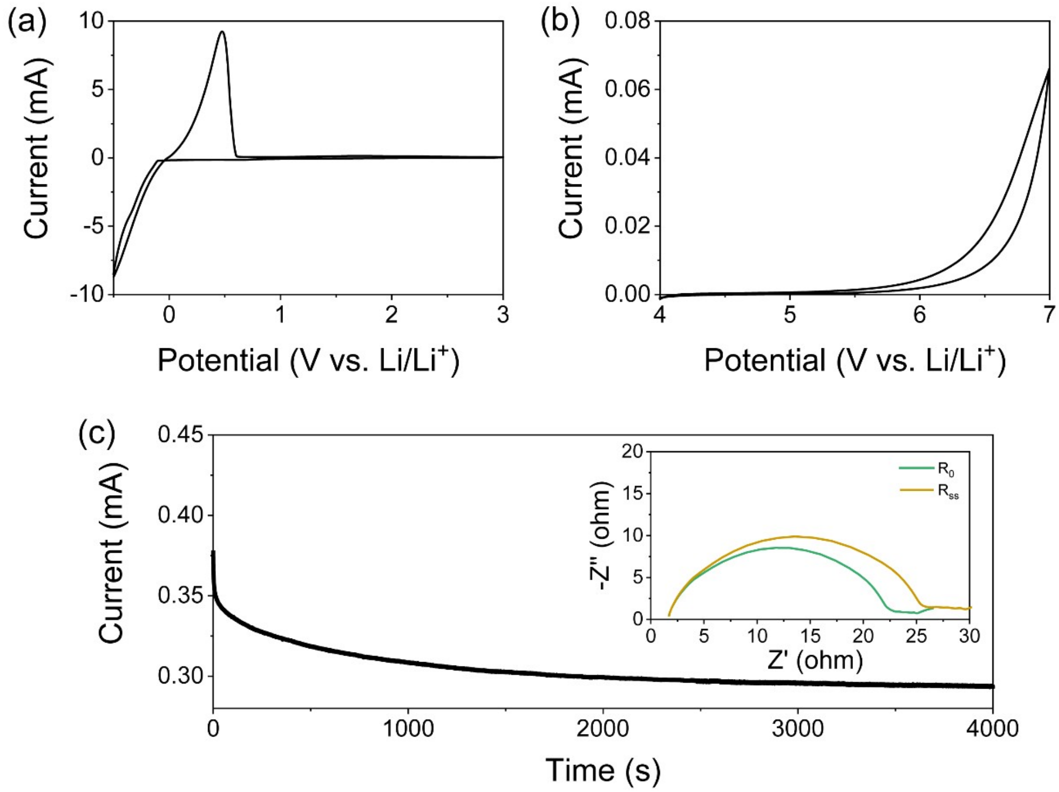

Figure S19. (a) Cathodic stability and (b) anodic stability of the electrolyte with the NFC/Al_2O_3 separator. (c) DC polarization curve of the Li//NFC/Al_2O_3//SS with insets showing the EIS Nyquist plots before and after polarization of the Li//NFC/Al_2O_3//Li cell.

As shown in Fig. S19, NFC/Al_2O_3 separator is relatively stable within the voltage range of 0-6 V, confirming that NFC/Al_2O_3 separator does not affect the electrochemical stability of the electrolyte [1,2].

The Li^+ transference numbers (t_{Li}) is measured using the Bruce-Vincent method [3]. t_{Li} is calculated according to:

$$t_{Li} = \frac{I_{ss}(\Delta V - I_0 R_0)}{I_0(\Delta V - I_{ss} R_{ss})}$$

where ΔV is the polarization voltage (10 mV), I_0 is the initial current (0.3769 mA), R_0 is the initial resistance (21.06 ohm), I_{ss} is the steady-state current (0.2936 mA), and R_{ss} is the steady-state resistance (24.25 ohm).

t_{Li} of the electrolyte with the NFC/Al_2O_3 separator was calculated to be 0.56, while the t_{Li} of pristine electrolyte is only 0.2-0.3 [4,5].

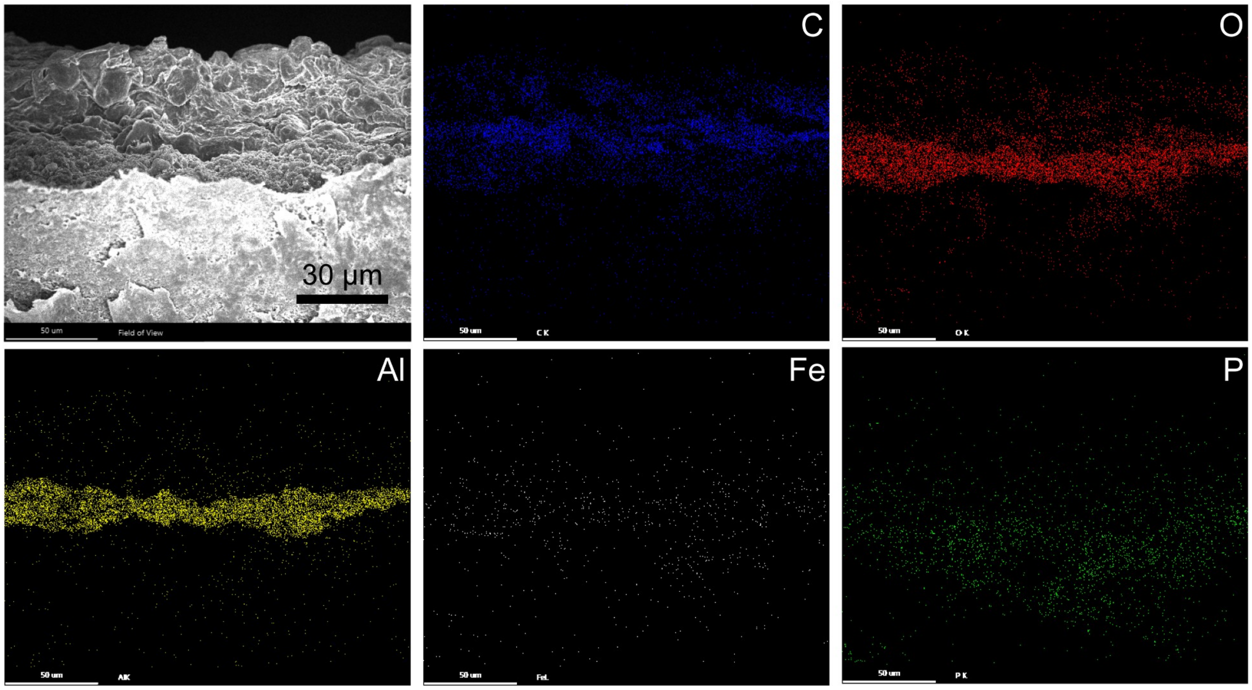

Figure S20. Cross-sectional SEM image of a sandwich-structured battery and the corresponding EDS elemental mappings.

References

[1] Xu, K., Ding, S. P., Jow, T. R. Toward reliable values of electrochemical stability limits for electrolytes. Journal of The Electrochemical Society, 1999, 146(11), 4172.

[2] Etacheri, V., Marom, R., Elazari, R., Salitra, G., Aurbach, D. Challenges in the development of advanced Li-ion batteries: a review. Energy & Environmental Science, 2011, 4(9), 3243-3262.

[3] Evans, J., Vincent, C. A., Bruce, P. G. Electrochemical measurement of transference numbers in polymer electrolytes. Polymer, 1987, 28(13), 2324-2328.

[4] Zhao, J., Wang, L., He, X., Wan, C., Jiang, C. Determination of lithium-ion transference numbers in LiPF6–PC solutions based on electrochemical polarization and NMR measurements. Journal of The Electrochemical Society, 2008, 155(4), A292.

[5] Mao, X., Shi, L., Zhang, H., Wang, Z., Zhu, J., Qiu, Z., Zhao, Y., Zhang, M., Yuan, S. Polyethylene separator activated by hybrid coating improving Li^+ ion transference number and ionic conductivity for Li-metal battery. Journal of Power Sources, 2017, 342, 816-824.